Earth and Planetary Science Letters 317-318 (2012) 282–294

Contents lists available at SciVerse ScienceDirect

Earth and Planetary Science Letters

journal homepage: www.elsevier.com/locate/epsl

The hafnium and neodymium isotope composition of seawater in the Atlantic sector of the Southern Ocean

Torben Stichel [a,*], Martin Frank [a], Jörg Rickli [b,1], Brian A. Haley [a,2]

[a] Leibniz Institute of Marine Sciences (IFM-GEOMAR), Wischhofstraße 1-3 in 24148 Kiel, Germany
[b] Institute of Geochemistry and Petrology, ETH Zürich, Clausiusstrasse 25, CH-8092, Switzerland

ARTICLE INFO

Article history:
Accepted 21 November 2011
Available online 28 December 2011

Editor: P. DeMenocal

Keywords:
hafnium
neodymium
seawater
Southern Ocean
radiogenic isotopes

ABSTRACT

We present the first combined dissolved hafnium (Hf) and neodymium (Nd) concentrations and isotope compositions of deep water masses from the Atlantic sector of the Southern Ocean. Eight full depth profiles were analyzed for Hf and twelve for Nd. Hafnium concentrations are generally depleted in the upper few hundred meters ranging between 0.2 pmol/kg and 0.4 pmol/kg and increase to relatively constant values of around 0.6 pmol/kg in the deeper water column. At the stations north of the Polar Front (PF), Nd concentrations increase linearly from about 10 pmol/kg at depths of ~200 m to up to 31 pmol/kg close to the bottom indicating particle scavenging and release. Within the Weddell Gyre (WG), however, Nd concentrations are essentially constant at 25 pmol/kg at depths greater than ~1000 m. The distributions of both elements show a positive correlation with dissolved silicon implying a close linkage to diatom biogeochemistry.
Hafnium essentially shows invariant isotope compositions with values averaging at $\varepsilon Hf = +4.6$, whereas Nd isotopes mark distinct differences between water masses, such as modified North Atlantic Deep Water (NADW, $\varepsilon Nd = -11$ to -10) and Antarctic Bottom Water (AABW, $\varepsilon Nd = -8.6$ to -9.6), but also waters locally advected via the Agulhas Current can be identified by their unradiogenic Nd isotope compositions. Mixing calculations suggest that a small fraction of Nd is removed by particle scavenging during mixing of water masses north of the PF. Nevertheless, the Nd isotope composition has apparently not been significantly affected by uptake and release of Nd from particles, as indicated by mixing calculations. A mixing envelope of an approximated North Pacific and a North Atlantic end-member shows that Nd isotope and concentration patterns in the Lower Circumpolar Deep Water (LCDW) can be fully explained by ~30:70 percentage contributions of these respective end-members.

1. Introduction

Radiogenic isotopes have been widely used to investigate present and past ocean circulation patterns, hydrothermal inputs, or continental weathering regimes (e.g. Albarède and Goldstein, 1992; Albarède et al., 1997; Frank et al., 1999; Piotrowski et al., 2000; van de Flierdt et al., 2002, 2004). In particular, neodymium (Nd) and hafnium (Hf) have oceanic residence times comparable to the global ocean mixing time and their radiogenic isotopes can therefore be used as tracers for water masses and their mixing (Godfrey et al., 2008; Lacan and Jeandel, 2005; Piepgras and Wasserburg, 1982; Rickli et al., 2009; Zimmermann et al., 2009a). The Nd and Hf isotope compositions are given in the ε-notation, which corresponds to the relative deviation of the $^{143}Nd/^{144}Nd$ and the $^{176}Hf/^{177}Hf$ of a sample from that of the CHondritic Uniform Reservoir (CHUR, $^{143}Nd/^{144}Nd = 0.512638$, Jacobsen and Wasserburg, 1980, $^{176}Hf/^{177}Hf = 0.282769$, Nowell et al., 1998) in parts per 10,000. The global average residence time of Nd is relatively well constrained at 500 to 2000 yrs (Jeandel et al., 1995; Tachikawa et al., 1999, 2003), although more recent estimates point to a somewhat lower number of <500 yrs (Arsouze et al., 2009; Siddall et al., 2008). However, despite the fact there have been numerous studies on the Nd isotope distribution in seawater, much of the global ocean, including the Southern Ocean, still remain unconstrained, which results in persisting uncertainties concerning the residence time and the biogeochemical cycling of Nd in seawater.

The global average residence time of Hf in seawater is even less certain with estimates ranging from 250 to 7500 yrs (Firdaus et al., 2008, 2011; Godfrey et al., 2008, 2009; Rickli et al., 2009; Zimmermann et al., 2009a). This uncertainty is mainly due to the lack of knowledge of the input sources and biogeochemical behavior of Hf in seawater, but also results from the sparse data available on dissolved Hf concentrations and isotope compositions of seawater. Nevertheless, a number of

* Corresponding author.
E-mail address: tstichel@hawaii.edu (T. Stichel).
[1] Now at Bristol Isotope Group, Department of Earth Sciences, University of Bristol, Parks Road, Bristol, United Kingdom.
[2] Now at COAS, Oregon State University, 104 Ocean Admin. Bldg., Corvallis, OR, 97331-5503, USA.

0012-821X/$ – see front matter © 2011 Elsevier B.V. All rights reserved.
doi:10.1016/j.epsl.2011.11.025

recent studies combining dissolved Hf and Nd isotope distributions from different areas of the global ocean have revealed similarities between the two radiogenic isotope systems with respect to distinct water mass signatures and their mixing (Rickli et al., 2009, 2010; Zimmermann et al., 2009a,b). These studies suggest that the lower end of the above estimates of the seawater residence time of Hf is more plausible.

Similar to Nd, Hf is thought to be supplied to the ocean mainly by continental weathering inputs (Bayon et al., 2006; Rickli et al., 2009, 2010; van de Flierdt et al., 2007). Previous work has suggested that the congruency of Hf isotope weathering may depend on the intensity of physical weathering on land, where intensified physical weathering potentially enhances the release of unradiogenic Hf from zircons (Piotrowski et al., 2000; van de Flierdt et al., 2002). A smaller variability in ε_{Hf} is observed in seawater compared to that of ε_{Nd} (Rickli et al., 2009, 2010; Zimmermann et al., 2009a,b). This is in contrast to crustal rocks, where the range in ε_{Hf} is about 50% larger than in ε_{Nd} (Patchett et al., 1984; Vervoort et al., 1999). The smaller variability of the Hf isotope composition in seawater could either indicate that incongruent weathering processes on land homogenize Hf isotopes before entering seawater (Bayon et al., 2006) or that Hf has a significantly longer oceanic residence time than Nd (Godfrey et al., 2008). Alternatively, potential hydrothermal inputs of radiogenic Hf from mid-ocean ridges, which are Nd sinks (Halliday et al., 1992), may at least partly be responsible for the observed isotopic range of dissolved Hf in seawater (Bau and Koschinsky, 2006).

In this study we present full water depth distributions of combined dissolved Hf and Nd isotopic compositions and concentrations in seawater samples from 14 sites in the Atlantic sector of the Southern Ocean. This study represents the first detailed investigation of the dissolved Nd and Hf isotope compositions of the water masses, as well as the biogeochemical cycling of the two elements in this key area of the global thermohaline circulation. Furthermore we investigate whether there are significant inputs of Hf and Nd from the Antarctic, as well as from the South American and African landmasses, which are characterized by a large range in types and ages of rocks and weathering regimes.

1.1. Hydrography

The hydrography of the study area and its variability have been subject of many detailed studies (e.g. Meijers et al., 2010; Orsi et al., 1995, 1999, 2002; Sievers and Nowlin, 1984; Stramma and England, 1999) and are only briefly summarized here. The circulation regime in the Atlantic sector of the Southern Ocean is dominated by the eastward flowing Antarctic Circumpolar Current (ACC), which is bounded to the north by the Subtropical Front (STF, Fig. 1). The major part of ACC essentially reaches from the surface to abyssal depths and is divided into Upper Circumpolar Deep Water (UCDW) and Lower Circumpolar Deep Water (LCDW) with neutral densities of $27.55\ kg/m^3 \leq \gamma^n \leq 28.27\ kg/m^3$ (Fig. 2). Another important current system in the Atlantic sector of the Southern Ocean is the cyclonically circulating Weddell Gyre (WG), which is located between the southern ACC boundary (BDY) and the Antarctic continent in the Weddell Sea (WS) (Fig. 1). The WG extends from the Antarctic Peninsula (AAP) to the Weddell–Enderby-Basin at about 20° E. The WG is fed by UCDW and LCDW from the ACC flowing in at intermediate depths, where it is then commonly called Warm Deep Water (WDW). Above WDW, Antarctic Surface Water (AASW) periodically gains density by brine rejection during sea ice formation. Along the continental slopes of

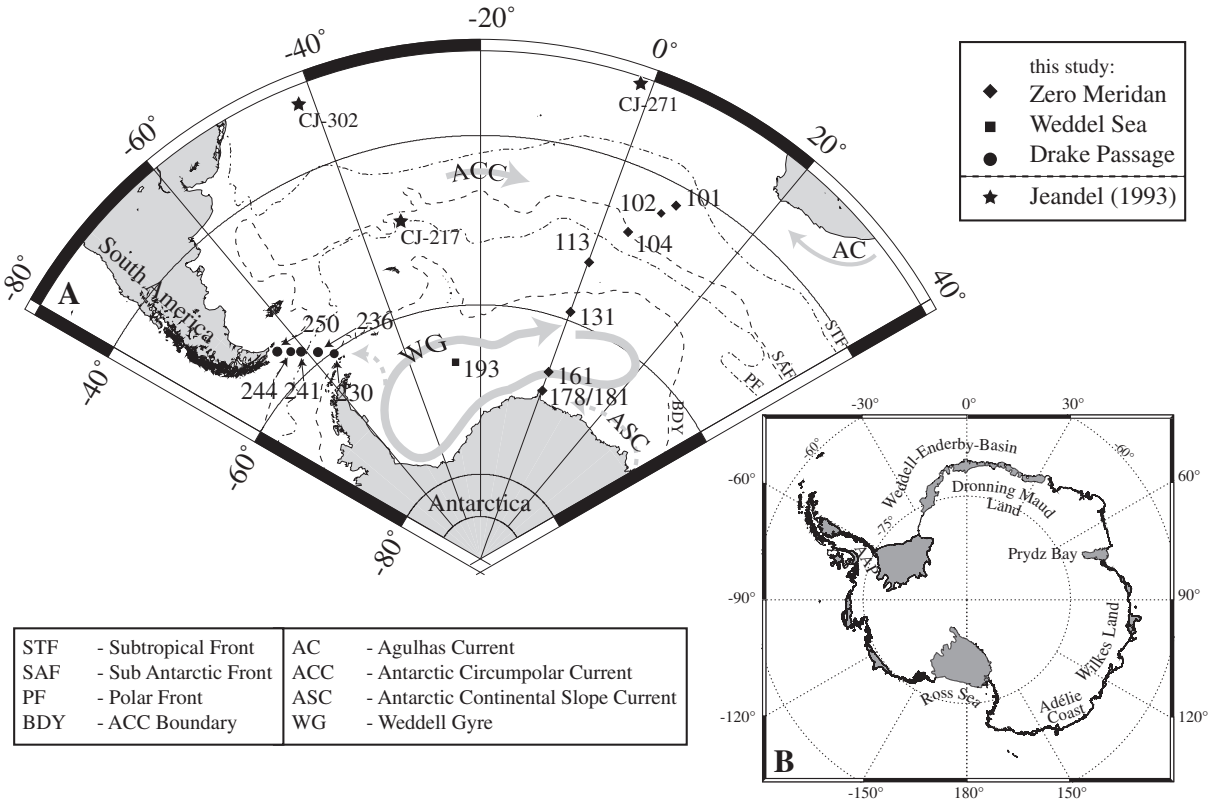

Fig. 1. (A) Sampling locations during expedition ANTXXIV/3 on the German research vessel *Polarstern*. The stations are grouped into three areas: The Zero Meridian comprising stations 101, 102, 104, 113, 131, 161, 178 and 181 (diamonds), the Weddell Sea (station 193, black square) and the Drake Passage (stations 230, 236, 241, 244 and 250, circles). Three further stations from Jeandel (1993) are indicated as stars. Gray arrows schematically indicate the direction of the Agulhas Current (AC) Antarctic Circumpolar Current (ACC) and the pathway of the Weddell Gyre (WG) the pathway of Bottom Waters are indicated in gray dashed arrows. The black dashed lines represent the approximate positions of the Subtropical Front (STF), the Polar Front (PF) and the southern ACC boundary (BDY) as provided by Orsi et al. (1995). (B) Overview map of the Antarctic continent with the relevant geographic regions and the extent of major ice shelves (gray shaded areas). AAP = Antarctic Peninsula.

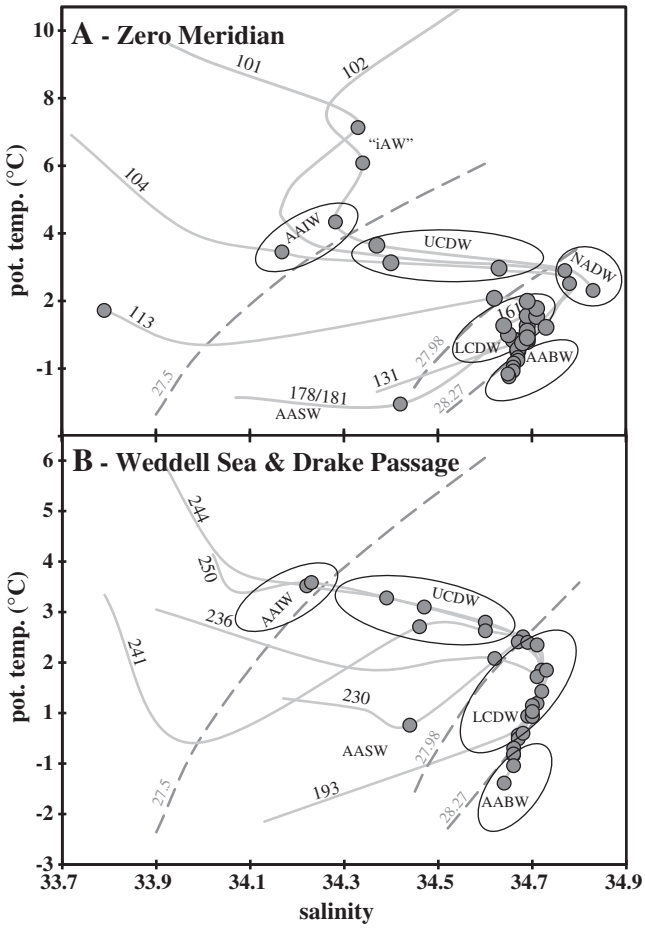

Fig. 2. Measured potential temperature versus salinity at the sampling stations along the Zero Meridian section (A) and through the Weddell Sea and the Drake Passage (B) provided by Rohardt (2009); doi:10.1594/PANGAEA.727465. The samples are grouped in water masses: Antarctic Intermediate Water (AAIW), "influenced by Agulhas Waters" ("iAW"), Upper Circumpolar Deep Water (UCDW) Lower CDW (LCDW), Antarctic Bottom Water (AABW) and North Atlantic Deep Water (NADW). The dashed lines indicate neutral densities (γ^n).

the WS these dense and cold surface waters sink down and mix with WDW. The part being dense enough to reach the bottom forms the Weddell Sea Bottom Water (WSBW), which is characterized by neutral densities of $\gamma^n \geq 28.40$ kg/m^3. These waters, however, are too dense to escape from the Weddell–Enderby Basin (Carmack and Foster, 1975). The less dense parts mix with WDW and feed into the Weddell Sea Deep Water (WSDW) directly, which is the densest water mass originating in the WS to permeate parts of the world ocean as AABW (28.40 kg/m$^3 \geq \gamma^n \geq$ 28.27 kg/m^3, e.g. Heywood and King, 2002; Klatt et al., 2005; Orsi et al., 1999, 2002 and references therein). About 60% of the AABW in the Southern Ocean forms in the western WS, whereas the remainder is produced in the Amery Ice shelf region, at the Adélie Coast and in the Ross Sea (Gordon, 1971; Orsi et al., 1999; Stramma and England, 1999). A recent study revealed that local AABW formation also takes place in further regions such as west of Prydz Bay (Meijers et al., 2010). Orsi et al. (1999) revisited the definition of AABW to point out that this water mass is not circumpolar due to its high density and is thus restricted to certain areas in the Atlantic sector, such as the Argentine Basin. The bottom water of southern origin that covers the remainder of the Atlantic sector of the Southern Ocean is less dense LCDW, often termed ACC bottom water (Orsi et al., 1999).

Another important water mass originating in the Southern Ocean is northward flowing Antarctic Intermediate Water (AAIW), marked by relatively high dissolved oxygen and low salinities with a neutral density range of 27.13 kg/m$^3 \leq \gamma^n \leq$ 27.55 kg/m^3 (Whitworth and Nowlin, 1987). AAIW originates from cooled surface waters of the ACC and is subducted northward at the Polar Front (Fig. 1). In the eastern Atlantic sector of the Southern Ocean AAIW is influenced by waters from the Indian Ocean, which are advected via the Agulhas Current (Roman and Lutjeharms, 2010; Stramma and England, 1999; Suga and Talley, 1995; Wüst, 1935).

Contributions from the north profoundly influence the water masses of the Southern Ocean. Southward flowing North Atlantic Deep Water (NADW) is separated into several branches at the northeastern tip of Brazil. A large fraction of NADW continues to flow eastward (Rhein et al., 1995), whereas the major part continues to flow southward into the southwestern Argentine Basin as part of the Deep Western Boundary Current. From here it is carried eastward within the ACC (Stramma and England, 1999). Along its pathway, NADW mixes with less dense waters returning from the southeast Pacific and the Indian Ocean to form UCDW but NADW is clearly identified by its characteristic deep salinity maximum within LCDW in the entire Atlantic sector of the Southern Ocean (Reid and Lynn, 1971).

2. Sample collection and analytical procedures

Samples from 14 stations were taken from a depth range between 200 m and 4800 m with Niskin bottles mounted onto a CTD-rosette during the expedition ANTXXIV/3 from February to April 2008 onboard the German research vessel *FS Polarstern* (Fig. 1). The expedition took place as part of the activities during the International Polar Year (IPY) 2008 and the chemical oceanographic investigations were part of the GEOTRACES program (SCOR Working Group, 2007). The stations are geographically grouped as follows: *Zero Meridian* (stations 101, 102, 104, 113, 131, 161, 178 and 181), *Weddell Sea* (station 193) and *Drake Passage* (stations 230, 236, 241, 244 and 250).

The samples were collected in acid-cleaned 20 l LDPE-collapsible cubitainers and volumes corresponded to 20 l for Nd and to 60 l for Hf. Each sample was filtered through a 0.45 µm Millipore® or Supor® filter within 12 h after collection. The samples were then acidified to pH ~2 using double distilled concentrated nitric acid. For each sample a filtered aliquot of 2 l was separated for the measurement of Hf and Nd concentrations. The large volume (60 l) samples for Hf isotope analysis were further processed on board by adding 100 mg of iron (Fe) to each 20 l cubitainer in the form of previously purified dissolved Fe–chloride ($FeCl_3$, for purification method see below). After allowing 24 h for equilibration, ammonia solution (25%, Merck-suprapur®) was added to bring the pH up to 8 inducing the co-precipitation of the dissolved Hf and Nd with the iron oxyhydroxides. After settling of the precipitate, most of the supernatant was discarded and the residue was transferred into 2 l PE-bottles for transport to the home laboratory.

The precipitates were then separated from the remaining supernatant by centrifugation and subsequently rinsed at least twice with MilliQ water to remove major ions. After the samples had been transferred into 60 ml Teflon vials, they were treated with 4 ml of aqua regia for at least 24 h at 110 °C to destroy organic components. Subsequently they were transferred into chloride by dissolution and evaporation in 4 ml of 6 M HCl. Another 4 ml of 6 M HCl was added to re-dissolve the samples. To separate the relatively large amount of Fe (300 mg) from the Hf a procedure similar to the one for cleaning the $FeCl_3$ solution was applied. This involves solvent extraction with 6 M HCl and purified di-ethyl ether in equal amounts, whereby Fe forms an ethereal complex and trace metals stay in the acidic phase (Nachtrieb and Conway, 1948; Nachtrieb and Fryxell, 1948). The sample solutions were then stirred to dissolve the iron in the ether, which finally contained more than 90% of the Fe and was removed by carefully siphoning the less dense Fe-ether complex from

Table 1
Sample locations, Hf and Nd isotope compositions and concentrations of Southern Ocean seawater samples together with hydrographic details.

	Depth (m)	Pot. T[a] (°C)	Salinity[a]	Neutral density	ε_{Nd}	Error (2 S.D.)	Nd (pMol)	ε_{Hf}	Error (2 S.D.)	Hf (pMol)	Si[b] (μMol)	Water mass (equivalent)
Station 101 (depth: 4670 m) 42° 20.60′ S 8° 59.20′ E	200	7.33	34.27	26.902	−8.3	0.39	8.47				4.39	AAIW
	500	5.59	34.34	27.222	−9.3	0.39	10.29				16.60	"iAW"
	750	3.83	34.28	27.393	−8.2	0.39	10.89	5.1	0.8	0.31	27.73	AAIW
	1000	3.15	34.37	27.555	−8.5	0.39	11.79				44.91	UCDW
	2000	2.45	34.77	27.963	−9.9	0.39	15.40				61.10	NADW
	3000	1.88	34.83	28.091	−10.9	0.39	20.21				64.32	NADW
	4400	0.72	34.73	28.204	−9.7	0.39	31.35				106.19	LCDW
Station 102 (depth: 4600 m) 44° 39.69′ S 7° 5.59′ E	200	6.63	34.33	27.065	−9.0	0.39	9.42	7.0	1.5	0.13	6.74	"iAW"
Station 104 (depth: 4550 m) 47° 39.80′ S 4° 16.20′ E	400	2.96	34.16	27.398	−8.4	0.39	10.26	6.7	1.5	0.23	27.54	AAIW
	750	2.63	34.40	27.644	−8.3	0.39	11.84	5.0	0.8	0.31	54.48	UCDW
	1200	2.47	34.63	27.847	−8.5	0.39	13.82	4.4	0.8	0.47	70.86	UCDW
	2000	2.08	34.78	28.027	−10.0	0.39	17.07	3.5	0.8	0.54	72.03	NADW
	4440	0.41	34.69	28.226	−8.7	0.39	27.91	4.4	0.8	0.62	120.45	LCDW
Station 113 (depth: 2530 m) 52° 59.80′ S 0° 02.00′ E	150	0.20	34.02	27.518	−8.0	0.39	15.01			0.21	50.39	UCDW/AAIW
	380	1.58	34.62	27.943	−8.3	0.39	16.37			0.42	87.75	UCDW
	550	1.49	34.69	28.025	−8.7	0.39	17.63			0.42	90.78	LCDW
	750	1.28	34.71	28.077	−8.6	0.39	19.48			0.40	98.19	LCDW
	1000	1.04	34.71	28.117	−8.4	0.39	20.60			0.48	103.36	LCDW
	1500	0.61	34.69	28.183	−8.6	0.39	22.70			0.46	115.47	LCDW
	2400	0.26	34.68	28.236	−8.5	0.39	24.51			0.50	127.57	LCDW
Station 131 (depth: 4600 m) 59° 00.00′ S 0° 00.00′ E	500	0.36	34.69	28.217	−8.6	0.39	23.71	4.1[c]	0.9	0.50	121.62	LCDW (WDW)
	1000	0.06	34.67	28.260	−8.4	0.39	25.30	4.2[c]	0.9	0.55	122.20	LCDW (WDW)
	1500	−0.12	34.67	28.292			25.94	3.8[c]	0.9	0.64	123.77	AABW (WSDW)
	2000	−0.30	34.66	28.326	−8.8	0.39	25.39				123.77	AABW (WSDW)
	2500	−0.42	34.66	28.348				4.7[c]	0.9		122.01	AABW (WSDW)
	3000	−0.53	34.66	28.369	−9.0	0.39	26.09			0.56	122.01	AABW (WSDW)
	3800	−0.69	34.65	28.401	−9.5	0.39	26.38	4.7[c]	0.9	0.58	117.52	AABW (WSBW)
Station 161 (depth: 4540 m) 66° 29.20′ S 0° 00.00′ E	200	1.06	34.69	28.088	−8.9	0.39	19.10			0.46	94.97	LCDW (WDW)
	440	0.77	34.69	28.146	−8.6	0.39	20.55	3.8	0.9	0.57	105.02	LCDW (WDW)
	800	0.52	34.69	28.196	−8.8	0.39	22.87	3.4	0.9	0.54	111.66	LCDW (WDW)
	1200	0.30	34.69	28.225	−8.5	0.39	24.29	4.8	0.9	0.58	120.93	LCDW (WDW)
	2400	−0.20	34.67	28.308	−8.7	0.39		4.4[c]	0.9	0.64	123.57	AABW (WSDW)
	3350	−0.42	34.66	28.348	−9.4	0.39	25.52				123.92	AABW (WSDW)
	4400	−0.57	34.65	28.378	−9.6	0.39	26.84	5.5	0.8	0.75	127.48	AABW (WSDW)
Station 178 (depth: 2000 m) 69° 23.00′ S 0° 00.00′ E	200	−1.55	34.42	27.981	−9.6	0.39	18.11				66.97	AASW
	500	0.50	34.65	28.105	−9.2	0.39	20.65				91.75	LCDW
	800	0.35	34.66	28.166	−9.1	0.39	22.22				100.34	LCDW
	1000	0.32	34.67	28.193	−8.9	0.39	23.30				106.29	LCDW
	1500	0.16	34.67	28.231	−9.0	0.39	24.49				114.69	LCDW
	1900	0.01	34.67	28.262	−9.0	0.39					118.30	LCDW
Station 181 (depth 1500 m) 69° 36.00′ S 0° 00.00′ E	1465	0.28	34.67	28.204	−8.6	0.30	23.76	4.5	0.8	0.50	110.88	LCDW (WDW)
Station 193 (depth: 4860 m) 66° 36.20′ S 27° 14.60′ W	500	0.44	34.69	28.197	−8.5	0.39	23.05			0.51	120.54	LCDW (WDW)
	1200	0.06	34.67	28.254	−8.8	0.39	25.03	3.2[c]	2.0	0.59	126.01	LCDW (WDW)
	2200	−0.29	34.66	28.323	−9.0	0.39	25.50	4.7[c]	1.1	0.65	125.62	AABW (WSDW)
	3200	−0.50	34.66	28.366	−8.9	0.39	26.10	4.0[c]	0.9	0.66	123.28	AABW (WSDW)
	4800	−0.84	34.64	28.429	−8.8	0.39	28.33	5.0[c]	0.9	0.67	123.67	AABW (WSBW)
Station 230 (depth: 3500 m) 60° 06.00′ S 55° 16.40′ W	250	0.26	34.44	27.894	−7.9	0.39	20.05				80.25	AASW
	400	1.91	34.67	27.956	−8.9	0.39	15.70				84.44	UCDW
	500	1.79	34.69	27.990	−8.2	0.39	17.59				86.93	LCDW
	1000	1.35	34.73	28.095	−8.2	0.39	19.87				101.15	LCDW
	1500	0.93	34.72	28.156	−8.3	0.39	24.92				112.45	LCDW
	2000	0.53	34.70	28.205	−8.0	0.39	24.59				121.58	LCDW
	2500	0.10	34.68	28.254	−8.2	0.39	25.59					LCDW
	3000	−0.13	34.66	28.286	−9.0	0.39	24.66				116.85	AABW (WSDW)
	3450	−0.28	34.66	28.312	−8.7	0.39	25.18				116.19	AABW (WSDW)
Station 236 (depth: 3770 m) 58° 59.60′ S 58° 08.60′ W	400	1.58	34.62	27.939	−8.4	0.39	16.12			0.46	83.32	UCDW
	1000	1.22	34.71	28.088	−8.6	0.39	19.14			0.58	99.67	LCDW
	1750	0.65	34.70	28.182	−8.2	0.39	21.52			0.61	115.97	LCDW
	2800	−0.01	34.67	28.267	−8.6	0.39	25.00			0.63	117.62	LCDW
	3712	−0.25	34.66	28.306	−8.5	0.39	25.34	4.8	0.9	0.70	117.17	AABW (WSDW)
Station 241 (depth: 3460 m) 57° 37.20′ S 60° 53.80′ W	480	2.21	34.46	27.752	−8.3	0.39	12.78	5.7	0.9	0.27	68.06	UCDW
	750	2.13	34.60	27.865	−8.5	0.39	14.20	4.3	0.9	0.44	78.31	UCDW
	1250	1.85	34.71	27.996	−8.6	0.39	16.38	5.4	0.9	0.51	89.97	LCDW
	2800	0.69	34.71	28.186	−8.3	0.39	23.81	4.7	0.9	0.64	120.47	LCDW
	3490	0.43	34.70	28.217	−8.5	0.39	25.30	3.5	0.9	0.60	121.21	LCDW
Station 244 (depth: 4170 m) 56° 53.80′ S 56° 55.14′ W	200	3.45	34.05	27.249	−8.1	0.39					13.66	AAIW
	500	3.02	34.22	27.453	−7.9	0.39	11.21				33.75	AAIW/UCDW
	750	2.78	34.39	27.617	−8.0	0.39	11.73				55.41	UCDW
	1250	2.30	34.60	27.846	−8.3	0.39	14.06				78.19	UCDW
	1750	1.90	34.69	27.968	−8.2	0.39					84.53	LCDW
	4100	0.45	34.70	28.215	−8.3	0.39	24.12				120.10	LCDW
Station 250 (depth: 3800 m) 55° 45.00′ S 64° 26.00′ W	500	3.08	34.23	27.458	−7.9	0.39	10.79	4.4	0.7	0.29		AAIW
	900	2.60	34.47	27.708	−8.4	0.39	12.14	4.2	0.6	0.40		UCDW
	1600	2.01	34.68	27.941	−8.0	0.39	15.14	4.4	0.6	0.54		UCDW

Table 1 (*continued*)

	Depth (m)	Pot. T[a] (°C)	Salinity[a]	Neutral density	ε_{Nd}	Error (2 S.D.)	Nd (pMol)	ε_{Hf}	Error (2 S.D.)	Hf (pMol)	Si[b] (μMol)	Water mass (equivalent)
Station 250 (depth: 3800 m) 55° 45.00′ S 64° 26.00′ W	2500	1.35	34.72	28.085	−8.0	0.39	19.76	4.7	0.6	0.58		LCDW
	3750	0.44	34.70	28.217	−8.4	0.39	24.40	4.2	0.6	0.64		LCDW

Errors are given as external errors.

[a] From the onboard scientific crew of the Alfred Wegener Institut (AWI), Bremerhaven, Germany (doi: 10.1594/PANGAEA.727465).

[b] From Fahrbach and de Baar (2010): The expedition of the research vessel *Polarstern* to the Antarctic in 2008 (ANT-XXIV/3).

[c] Values with higher ^{176}Yb contribution on ^{176}Hf than 0.3% and therefore a manual correction was applied.

the acidic phase. This procedure was repeated to remove most of the residual Fe.

Many samples formed jelly-like precipitates in 6 M HCl, containing ~90% of the Hf from the samples. These precipitates were separated by centrifugation and subsequently dissolved in 2 M HF. After evaporation the supernatant from the jelly precipitate was admixed again to each sample. Due to remaining small amounts of calcium and magnesium in the samples, occasionally fluoride precipitates formed, which were re-dissolved in a mixture of 6 M HCl and 0.3 M boric acid. Hafnium was then separated from the main matrix including Nd through cation exchange chromatography (1.4 ml resin bed, BIORAD® AG50W-X8, 200–400 μm mesh-size). The samples were loaded in 0.5 ml 1 M HCl/0.05 M HF, and Hf was eluted adding another 2 ml of the same reagent. Neodymium was collected in 6 ml 8 M HNO_3 after washing out the main part of the cation matrix and the remaining iron with 5 ml of 3 M HCl. The Nd cuts were kept as a backup for the actual 20 l Nd isotope samples. The Hf-cuts were further purified following a slightly modified separation scheme of Münker et al. (2001). The total procedural blank for Hf was negligible at 15 pg to 20 pg compared to typical sample sizes of 4 ng to 5 ng.

The 20 l Nd aliquots were shared samples and were initially processed at AWI since thorium (Th) and protactinium (Pa) had to be separated first, because measurement of the ^{231}Pa concentration required addition of a short-lived ^{233}Pa spike (see Venchiarutti et al., 2011). The rare earth elements (REEs) including Nd were separated from Th and Pa using an anion exchange resin (BIORAD® AG1-X8, 100–200 μm mesh-size) following the procedure described in Venchiarutti et al. (2008). Iron was subsequently separated from the REEs by solvent extraction at IFM-GEOMAR in Kiel, as outlined for Hf above. Further purification of the REEs was achieved through cation exchange chromatography (0.8 ml resion bed, BIORAD® AG50-X12, 200–400 μm mesh-size), whereby major cations were removed first and the REEs were then eluted in 6 M HNO_3. Neodymium was finally separated from Sm and the other REEs on 2 ml LN-Spec resin (EICHROM®, Pin and Zalduegui (1997)). The total procedure blank for Nd was lower than 30 pg, and thus negligible.

2.1. Hf and Nd concentration measurements

The Hf and Nd concentrations were obtained by isotope dilution (ID) following Rickli et al. (2009). Previously weighed ^{178}Hf-single spike and ^{150}Nd/^{149}Sm double-spike solutions were added to an acidified 0.5 l aliquot of each sample. The samples were left for 4 to 5 days for complete isotopic equilibration. $FeCl_3$ solution was added to the samples and Hf and Nd were co-precipitated with iron hydroxides by adding ammonia to raise the pH to 8. The purification of Hf and Nd was sufficient for subsequent mass spectrometric analysis using a single cation chromatographic separation step (1.4 ml resin bed, BIORAD® AG50W-X8, 200–400 μm mesh-size). The respective cuts containing Nd and Hf were evaporated to dryness and then oxidized by adding 200 μl of a 1:1 mixture of 0.5 M HNO_3 and H_2O_2 (30 wt.%) to reduce disturbing matrix effects of organic components during measurement on the MC-ICPMS. Replicates for each element were processed and yielded an external reproducibility of better than 1% for Nd and between 3 and 10% for Hf depending on concentration. The procedural blanks were quantified by processing 0.5 l of MQ-water in the same way as the samples and corresponded to less than 1% in the case of Nd, for which no blank corrections were applied. The Hf content of the samples was closer to the blank level. The blank corresponded to 5 ± 0.7 pg ($n = 11$), which was then subtracted from the samples to achieve a correct seawater concentration.

2.2. Hf and Nd isotope measurements

The Hf isotope compositions were measured on a *Nu Plasma HR MC-ICPMS* at IFM-GEOMAR in manual time resolved mode due to the low Hf concentrations of the samples. The samples were dissolved in 250 to 500 μl 0.5 M HNO_3/0.1 M HF to obtain Hf concentrations of approximately 20 ppb corresponding at total beam of at least 4 V. The measured isotope ratios were integrated over the time of analysis with a typical total duration between 3 and 5 min. The measured Hf isotope compositions were corrected for instrumental mass bias to ^{179}Hf/^{177}Hf = 0.7325 applying an exponential mass fractionation law. The JMC 475 standard was measured during each session of 2 to 6 samples and all ^{176}Hf/^{177}Hf ratios presented here were normalized to the accepted literature value of 0.28216 (Nowell et al., 1998). The external reproducibility ranged from ± 0.6 ε_{Hf} to ± 2.6 ε_{Hf} (2 S.D.) depending on sample size and was estimated by repeated measurements (4 to 6 times each session) of both the JMC 475 standard and a certiPUR® ICPMS Hf-standard.

Most of the samples showed little remaining ytterbium (Yb) (<0.3% of the ^{176}Hf beam in the purified Hf) and corresponding interferences on ^{176}Hf were readily correctable following Chu et al. (2002). For some samples the Yb corrections were larger and corresponded to up to 2.2% of the ^{176}Hf beam. In order to avoid losing Hf during repeated chromatographic separation, those data were corrected applying an offset correction obtained from a series of Yb-doped JMC475 standards similar to Kemp et al. (2009). The systematic change in the Hf isotope composition of these standards depending on the amount of added Yb was linear ($R^2 = 0.971$) and the method was therefore considered reliable. The samples, which were corrected by this approach, are marked with a superscript "c" in Table 1.

The Nd isotope composition was either measured on a *Thermo Scientific TRITON 1 TIMS* or on the *Nu Plasma* at IFM-GEOMAR depending on the amount of Nd available for each sample. The smallest samples (<20 ng) were measured in time-resolved mode on the *MC-ICPMS*. The measured isotopic composition was corrected for instrumental mass bias using ^{146}Nd/^{144}Nd = 0.7219 applying an exponential mass fractionation law. The ^{143}Nd/^{144}Nd ratios were normalized to the accepted value for the JNdi-1 standard of 0.512115 (Tanaka et al., 2000). The external reproducibility on both instruments was between ± 0.3 and ± 0.4 ε_{Nd} units (2 S.D.) estimated by repeatedly measuring JNdi-1 and an internal laboratory standard, with $n = 4$–6 during each measuring session. Replicates measured on both mass spectrometers resulted in identical Nd isotope compositions within analytical error.

3. Results

3.1. Hf and Nd concentration

Both elements show concentration patterns similar to most particle reactive metals in that lowest concentrations are observed in near surface waters (down to ~500 m depth, Figs. 3 and 4). Concentration minima in this shallow depth interval occur at stations near and north of the PF (stations 101, 104, 113, 241, 244 and 250) with 0.21 pmol/kg to 0.29 pmol/kg for Hf and 8.5 pmol/kg to 16.4 pmol/kg for Nd. These stations also exhibit the strongest increase in concentration with depth for both elements. However, the slope of the increase differs between Hf and Nd. The Hf concentrations only increase significantly with water depth within the upper 500 m to 1000 m and are more or less constant at greater depths resulting in a nutrient-like pattern. In contrast, Nd concentrations increase almost perfectly linearly with water depth ($R^2 > 0.93$). The stations in the WG (stations 131, 161, 178 and 193) show only minor increases with water depth for both elements. The highest concentrations are generally measured in deepest waters with Hf and Nd concentrations up to 0.75 pmol/kg (station 161) and 31.35 pmol/kg (station 104), respectively. The Hf concentration patterns for stations 131 and 241 are different, in that they show mid depth maxima at 1500 m (0.64 pmol/kg) and 2800 m (0.64 pmol/kg), respectively and slightly lower concentrations deeper (Fig. 3). The concentrations of both elements correlate well with dissolved silicon (Si, Middag et al., 2011) yielding an R^2 of 0.73 for Hf and 0.87 for Nd (Fig. 5). Any potential increase in Hf concentration at station 113, where hydrothermal activity left a strong imprint on the Fe and manganese (Mn) concentrations at depths between 1500 and 2000 m (Klunder et al., 2011; Middag et al., 2011), was not observed.

3.2. Hf isotope distribution

The Hf isotope compositions of the entire sample set show remarkably little deviation from an average $\varepsilon_{Hf} = +4.6$ (Fig. 3). The three most distinct samples yield a range of ε_{Hf} between a minimum of +3.2 and maxima of +6.7 and +7.0. These samples, however, also have the poorest external reproducibility between ±1.5 and ±2 ε_{Hf} (2 S.D.) due to only trace amounts of available Hf. All other samples have much lower uncertainties (0.5 to 1 ε_{Hf} units) but do not reveal significant variations outside these statistical uncertainties. In addition, those samples that needed larger Yb interference corrections (see Section 2.2) are consistent with the rest of the dataset proving that these corrections are accurate.

3.3. Nd isotope distribution

The Nd isotope data in this study range from $\varepsilon_{Nd} = -7.9$ to $\varepsilon_{Nd} = -10.9$ (Fig. 4, Table 1). In the Drake Passage (DP) only small variations between $\varepsilon_{Nd} = -8.6$ and −7.9 are observed. The only station in the Weddell Sea (WS, 193) yields an average Nd isotope composition of $\varepsilon_{Nd} = -8.8$ and no significant variations with water depth. The eight stations from the Zero Meridian (ZM) and its vicinity show variations between $\varepsilon_{Nd} = -10.9$ and −8.4, whereby the least radiogenic values were measured at stations 101 (2000 m and 3000 m, $\varepsilon_{Nd} = -9.9$ and −10.9, respectively) and 104 (2000 m, $\varepsilon_{Nd} = -10.0$), which coincide with the salinity maximum of NADW (Fig. 2, Table 1).

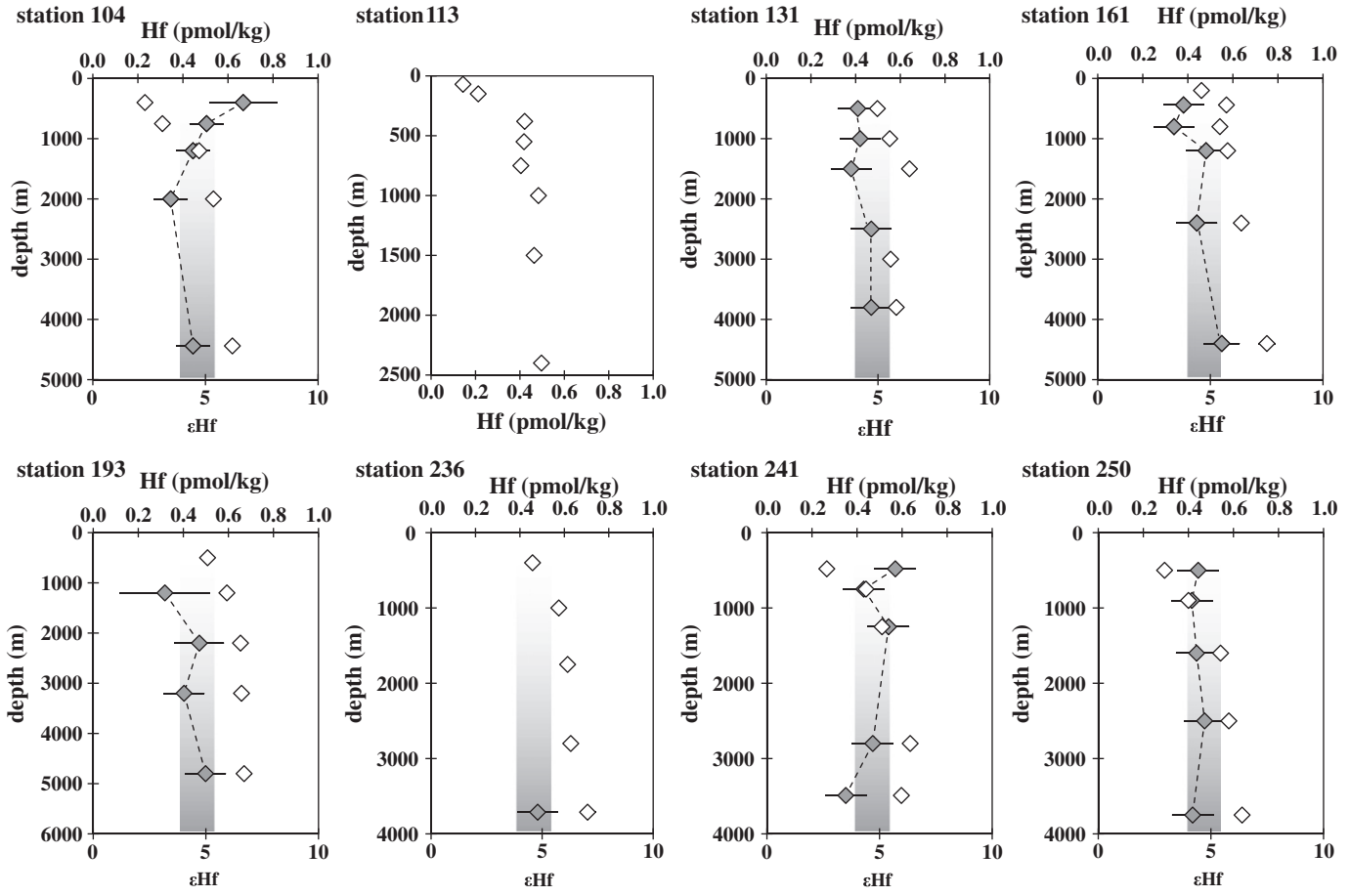

Fig. 3. The Hf concentration (open diamonds) and isotopic composition (solid diamonds) as a function of depth at the sampled stations. Error bars for the isotopic composition represent 2 S.D. (external). Analytical errors for the concentrations are smaller than symbol size. Stations 101, 102 and 181 are omitted in this figure, because only one Hf isotope value of each station was obtained (see Table 1). The gray bar marks the average Hf isotope composition of the entire sample set.

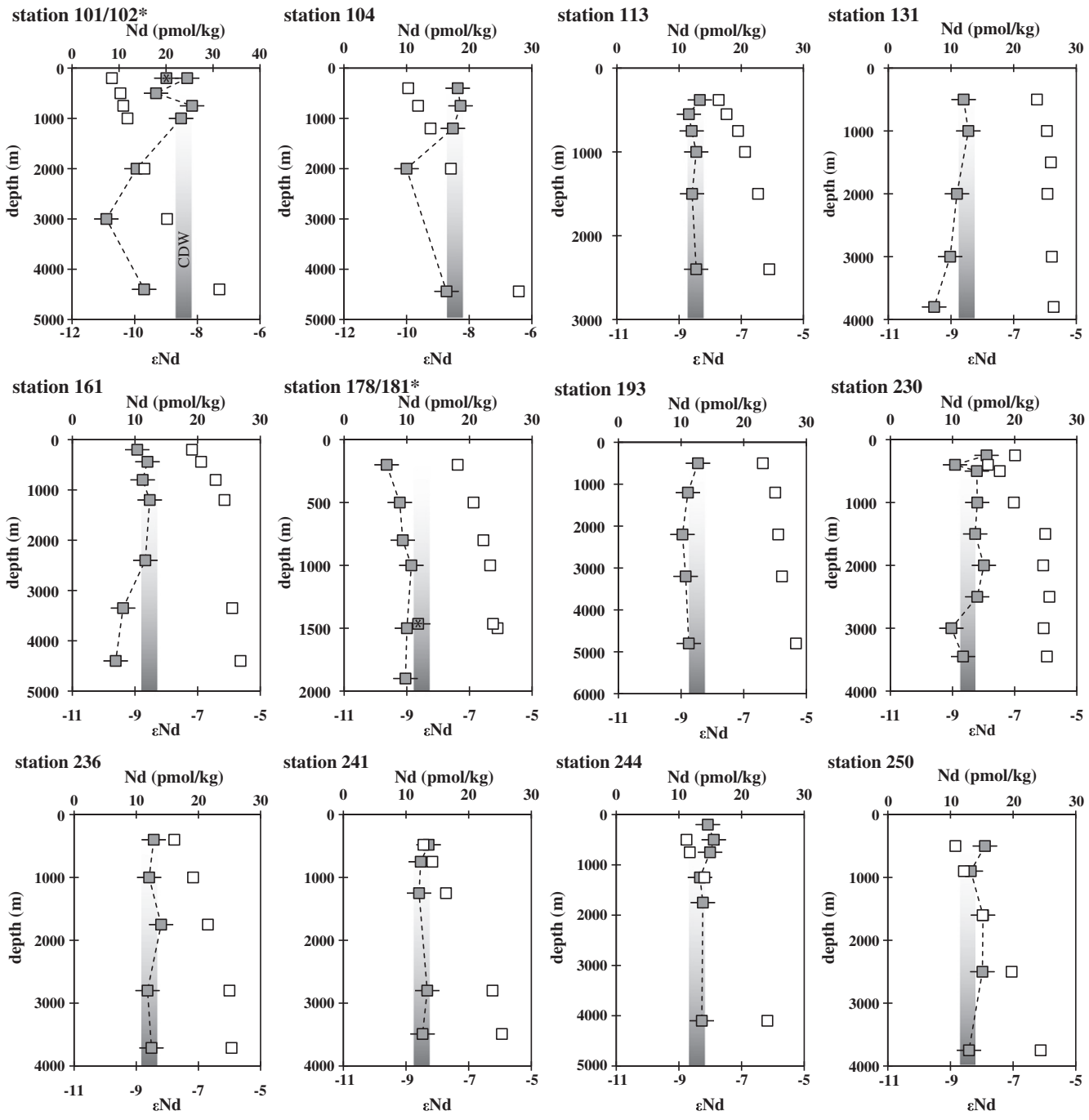

Fig. 4. The Nd concentration (open squares) and isotope composition (solid squares) as a function of depth at the sampled stations. Error bars for the isotopic composition represent 2 S.D. (external). Analytical errors for the concentrations are smaller than symbol size. Single samples from stations 102 and 181 are combined at stations 101 and 178, respectively and are indicated as crosses. The gray bar marks the mean Nd isotope value of CDW for the entire sample set.

The overall Nd isotope composition of AABW averages at $\varepsilon_{Nd} = -9.0$ (± 0.4, 1 S.D., variations within a water mass are reported as 1 S.D.), whereby the deepest samples of stations 131 and 161 ($\varepsilon_{Nd} = -9.6$ and $\varepsilon_{Nd} = -9.5$, respectively) are the least radiogenic ones. Samples from within AAIW average at $\varepsilon_{Nd} = -8.1$ (± 0.2). The values obtained at stations 101 ($\varepsilon_{Nd} = -9.3$) and 102 ($\varepsilon_{Nd} = -9.0$) were sampled within shallow local salinity maxima of the respective profiles, which suggests an influence from the Agulhas current and which are here referred to as "influenced by Agulhas Water" ("iAW") (Boebel et al., 2003; Roman and Lutjeharms, 2010, E. Fahrbach, pers. comm.). The two uppermost samples of stations 178 and 230 correspond to AASW, and yielded $\varepsilon_{Nd} = -7.9$ and -9.6, respectively. Most Upper and Lower CDW samples are isotopically indistinguishable from each other with average values of $\varepsilon_{Nd} = -8.4$ (± 0.2) and $\varepsilon_{Nd} = -8.6$ (± 0.2), respectively. The only exceptions are observed at station 178 close to the Antarctic continent, where LCDW is on average less radiogenic ($\varepsilon_{Nd} = -9.0 \pm 0.1$) and at station 101 (4400 m, $\varepsilon_{Nd} = -9.7$).

4. Discussion

4.1. Processes controlling Hf and Nd concentrations in the Southern Ocean

The distribution of the concentrations for both elements shows correlations with those of dissolved nutrients such as Si (Fig. 5) or phosphate (not shown here). In particular at the Polar Frontal Zone

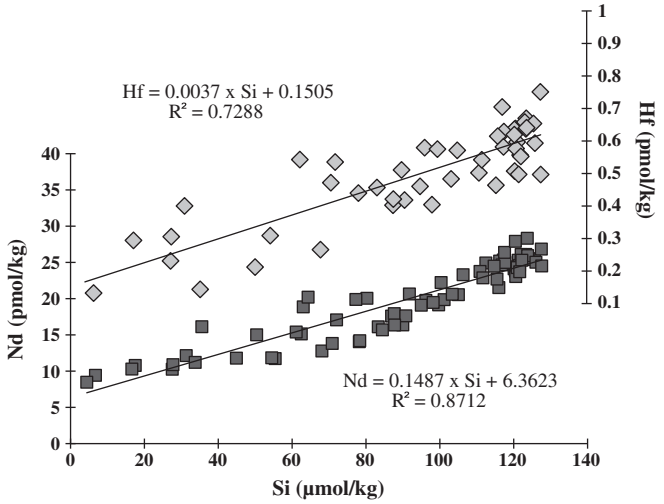

Fig. 5. Concentrations of Hf (gray diamonds) and Nd (black squares) versus dissolved silicon (Fahrbach and de Baar, 2010 and Middag et al., 2011). Neodymium yields a better correlation with dissolved Si than Hf, indicating a higher release from the frustules of diatoms in the Southern Ocean.

(between the PF and the SAF) where nutrients are upwelling and are consumed quickly, the subsurface concentrations of Hf and Nd (and the nutrients) are significantly lower than at all other stations. Dissolved Hf and Nd, similar to other trace metals, are most likely scavenged onto the relatively large specific surface areas of diatoms, as already suggested by Rickli et al. (2009). The diatom frustules and the organic matter sinking down from the surface waters dissolve, which leads to release of the previously scavenged trace metals. In fact, modeling studies by Sarmiento et al. (2007) have shown that the Southern Ocean is the most important area of the global ocean for opal dissolution. Thus, the close correlation of Hf and Nd concentrations with dissolved Si concentrations shown in Fig. 5 most likely reflects the release of Hf and Nd from dissolving diatom frustules. The better correlation of Nd with dissolved Si ($R^2 = 0.87$) than that of Hf ($R^2 = 0.73$) suggests that Nd, after being removed from the mixed layer through adsorption to and incorporation into diatoms is more readily released again when these frustules dissolve. Samples taken in the upper 500 m near or at the PF (stations 104, 113, 241 and 250; Figs. 3 and 4), where productivity and thus particle density are highest (e.g. Rutgers van der Loeff and Berger, 1993; Venchiarutti et al., 2011), all show low Hf and Nd concentrations indicating efficient removal in this depth interval. Toward 500 m water depth Hf concentrations increase and remain rather constant below (Fig. 3) suggesting that Hf remineralization is already complete in shallow waters. This implies an overall less efficient remobilization from sinking particles and thus a more efficient removal from the water column. This contrasts with Nd, for which the increase in concentration from near the surface to the seafloor is quasi linear at these stations (Fig. 4) suggesting a steady release and desorption during opal dissolution. However, in particular for Nd, the concentration patterns change toward the south (stations 131, 161, 178, 193 and 230) to a more nutrient like pattern. There, although slightly higher than further north, near surface concentrations are still depleted and increase toward 500–1000 m depth. Below that depth the concentrations remain fairly constant, implying reduced remineralization for both elements. Based on Th and Pa distributions, Rutgers van der Loeff and Berger (1993) have shown that south of the ACC (i.e. in the WG) particle flux is largely reduced. Our inferences are consistent with this conclusion, in that all stations within the WG (131, 161, 178 and 193) and also in the southern DP at station 230 show rather consistently higher concentrations of both Hf (0.4 pmol/kg to 0.75 pmol/kg) and Nd (19 pmol/kg to 28 pmol/kg). Significantly lower concentrations at these stations are only found in the upper 1000 m again indicating that remineralization for Nd and Hf is completed within the upper water column. Inverse modeling of particulate export and opal fluxes also points to such shallow remineralization in the Weddell Sea (Usbeck et al., 2002). In fact, studies on trace metals, such as micronutrients Fe (Klunder et al., 2011) or zinc (Baars and Croot, 2011) carried out on the same expedition (ANTXXIV/3) show similarities in the Hf and Nd in concentration patterns. Specifically, both micronutrients are consumed efficiently in the mixed layer (~200 m) in more productive waters (i.e. north of the PF) and are regenerated more or less continuously throughout the water column. Within the WG shallow remineralization of Fe and Zn similar to Nd and Hf is observed (Baars and Croot, 2011; Klunder et al., 2011), further supporting that Hf and Nd concentrations are strongly controlled by uptake and release of biogenic particles in the Southern Ocean.

If diatom growth is indeed a sink term for Hf, then the oceanic residence time of Hf should be shorter than that of Nd, at least in areas where diatoms are the prevailing primary producers. A similar effect of removal is also observed for Pa (Yu et al., 1996). These authors documented an ~50% removal of Pa exported from the North Atlantic due to scavenging on biogenic opal. In dissolved form both, Hf and Pa, mostly exist in OH-complexes (e.g. Byrne, 2002) and have therefore potentially a similar scavenging behavior in seawater. In fact, a pronounced concentration decrease of up to ~50 and at least 25% is observable by comparing deep (deeper than 1000 m) Hf concentrations in the Atlantic (~1 pmol/kg, Rickli et al., 2009) and the ones in the Southern Ocean (0.21 to 0.75 pmol/kg, this study). A shorter oceanic residence time of Hf than that of Nd has already been proposed by Rickli et al. (2009) and Zimmermann et al. (2009a) based on the fact that the Hf concentration gradient from the Atlantic (~1 pmol/kg, Rickli et al., 2009) to the Pacific (~0.5 pmol/kg, Zimmermann et al., 2009a) is opposite to that of Nd, implying no enrichment of Hf with age of deep waters and thus supporting a short residence time. However, the small vertical gradient in Hf concentration observed in our Southern Ocean data can also be interpreted to reflect a longer residence time of Hf compared to Nd: The cessation of increase in Hf concentrations below 500 m water depth may imply an already completed re-dissolution from the sinking particles, and thus a sooner release of Hf than of Nd. In addition, also the fairly similar Hf concentrations in the Atlantic and the Pacific may reflect a long residence time for Hf, rather than a lack of Hf enrichment along the deep ocean conveyer. Both scenarios are plausible but result in opposite interpretations. Therefore, a conclusion about the relative residence time cannot be made on the basis of our concentration data alone.

4.2. Hf isotope distribution in Southern Ocean water masses

The isotopic composition of Hf is essentially invariable throughout the entire sample set given that most observed isotopic compositions are indistinguishable from the average value of $\varepsilon_{Hf} = +4.6$ (Table 1, Fig. 3). Distinction of water masses on the basis of their Hf isotope compositions in the Southern Ocean is therefore not possible at the currently achievable external reproducibility of the data and means that Hf isotopes are not a useful water mass tracer in this area. In contrast to Nd (see Section 3.3), no distinguishable NADW or AABW isotopic signature is observed (Fig. 3). This isotopic homogeneity in Hf supports a longer residence time for Hf than for Nd. However, the observed invariance in Hf isotopes in the Southern Ocean may also be compatible with a shorter residence time for Hf than for Nd given the weak isotopic gradient in Hf isotopes between the surrounding ocean basins. The data available so far show a difference in Hf isotope compositions between the deep Pacific Ocean (Zimmermann et al., 2009a) and the deep Atlantic Ocean (Rickli et al., 2009) of only 3 to 4 ε_{Hf} units, which is small relative to that of Nd isotopes (9 to 10

ε_{Nd} units) and is thus easier to homogenize within the ACC. Whether the homogenous Hf isotope composition in global seawater, as well as in the ACC, is a result of homogenization (long residence time) or already preset due to incongruent weathering cannot be decided with the currently available data. To resolve this issue, more studies on the input mechanisms and input signatures of dissolved Hf to seawater need to be carried out in the future. So far, only a few studies (Bayon et al., 2006; Rickli et al., 2010) have addressed this topic and the resulting picture is not conclusive.

Compared to these modern data, paleo-records however do show some variations: Hafnium isotope data obtained from ferromanganese nodules indicate that AABW incorporated an isotopic fingerprint of Wilkes Land in East Antarctica (ε_{Hf}~3, van de Flierdt et al., 2006), which implies an unradiogenic Hf input from the Antarctic continent. In our study area, we do not observe such an imprint on the Hf isotope composition of AABW, and therefore conclude that AABW in the Atlantic sector currently does not receive distinguishable amounts of isotopically different Hf from the Antarctic shelf, despite the fact that the Hf isotope range of ~30 ε_{Hf}-units along the shelf is large (van de Flierdt et al., 2007). Either the Hf contributions from the Antarctic continent are too small to be distinguished in the water column or the Hf isotope compositions released from incongruent weathering are similar to the signatures of CDW. Alternatively, there may have been changes in Antarctic continental inputs in the past, which influenced the paleo-AABW signal, given that the data obtained from ferromanganese nodule surface scrapings (van de Flierdt et al., 2006) integrate over several 10,000 to 100,000 yrs.

4.3. Nd isotope characteristics of Southern Ocean water masses

The overall Nd isotope composition of the water masses in the Atlantic sector of the Southern Ocean exhibits only small but resolvable differences, probably due to the efficient horizontal and vertical homogenization within the ACC and the WG (Fig. 6). The average circulation time of a parcel of water in CDW around Antarctica is only about 50 to 70 yrs (Georgi, 1981), which is far shorter than the average oceanic residence time of Nd of at least several hundred years (Arsouze et al., 2009; Jeandel et al., 1995; Siddall et al., 2008; Tachikawa et al., 1999, 2003). However, the Nd isotope distribution in the study area allows distinguishing between northern (i.e. NADW) and southern (i.e. AABW) sourced water masses (Fig. 6A).

4.3.1. Nd isotope composition of intermediate waters

The AAIW ($\varepsilon_{Nd} = -8.4$ to -7.9) has the most radiogenic Nd isotope composition observed in the Atlantic sector of the Southern Ocean in this study. More radiogenic values for AAIW of up to $\varepsilon_{Nd} = -6.2$ and -6.8 also reported from the South Atlantic (Jeandel, 1993, Fig. 1),

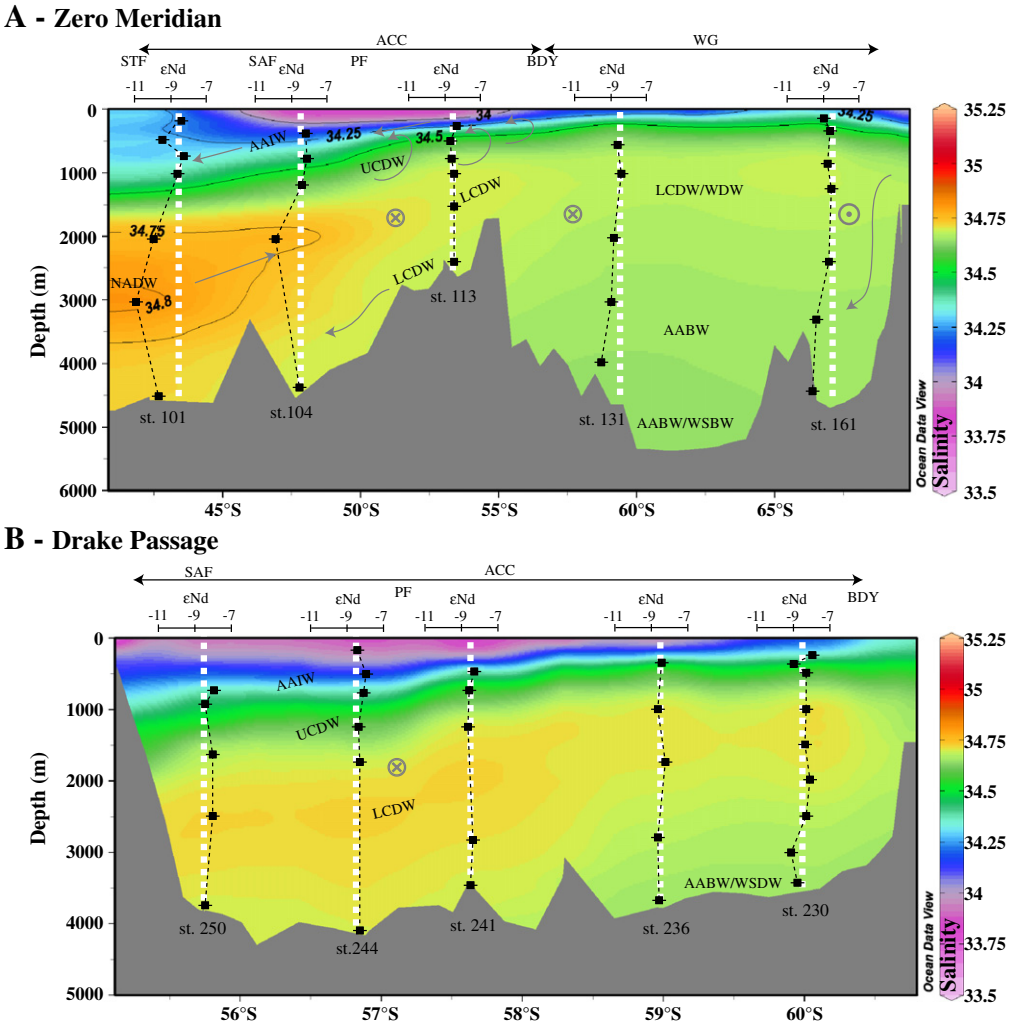

Fig. 6. The Nd isotope distribution along the Zero Meridian (A) and across the Drake Passage (B). Crosses mark predominant eastward flow directions and the point symbol denotes westward flow. The color scales represent the salinity distribution of each section. Approximate positions of major water masses described in Section 1.1 are indicated by their respective acronyms. This figure is made using Ocean Data View (Schlitzer, 2011).

which may indicate an even higher Pacific contribution to AAIW supplied through the DP, are not reproduced here. In the DP all five profiles from our study do not show any significant shifts to comparably radiogenic values (Fig. 6B). This does not support Pacific waters being responsible for the highly radiogenic values of AAIW data observed by Jeandel (1993, stations from therein are indicated as black stars in Fig. 1). However, station 271 from Jeandel (1993) was sampled close to the South Sandwich Islands, which consists of volcanic island arc rocks (Fig. 1). These relatively young mafic rocks and weathered deposits around the islands may have shifted the Nd isotope composition toward more radiogenic values. For the station in the SE-Atlantic (St. 217, Fig. 1) Jeandel (1993) measured a value of $\varepsilon_{Nd} = -6.2$ for eastern south Atlantic AAIW, which is not explainable by a potential influence from the South Sandwich Islands due to the large distance. An alternative interpretation may be advection of intermediate waters from the Indian Ocean, e.g. via the Agulhas Current, which is, however, not supported by our new data set: At stations 101 (500 m) and 102 (200 m) even less radiogenic ε_{Nd} values of −9.3 and −9.0 compared to CDW were measured, implying a contribution of waters other than the Southern Ocean in origin. These stations are located in an area where the Agulhas Current (AC) feeds South Atlantic waters (Boebel et al., 2003; Roman and Lutjeharms, 2010, E. Fahrbach pers. comm.), which is clearly delineated by local salinity maxima at these depths. Thus the AC carries an unradiogenic Nd isotope signature in the area of the Agulhas retroflection. A rather unradiogenic composition of the AC is also supported by surface sediments signatures, being as low as $\varepsilon_{Nd} = -15.5$ to −11 (Franzese et al., 2006) in the area of the southeastern margin of South Africa and there is also no indication for a radiogenic AAIW signal in the northern Cape Basin at 25° S where Rickli et al. (2009) measured an $\varepsilon_{Nd} = -11$ for AAIW. The observed discrepancy of the Nd isotope signatures in AAIW between our data set and stations 217 and 271 of Jeandel (1993) can therefore not be satisfactorily explained at present.

The overall similarity of the Nd isotope composition of AAIW and CDW in our data set confirms efficient vertical and horizontal homogenization in the Southern Ocean. Upwelling CDW comes close to the surface near the Antarctic continent and is then advected north where it eventually sinks at the PF to form AAIW. Along this pathway no significant change in the Nd isotope composition is observed in our data, arguing against any further addition of Nd with a different isotope composition to these waters before they are subducted near the PF.

4.3.2. Nd isotope composition of AABW

Despite the generally small isotopic variability in the Southern Ocean, the water column Nd isotope data show that the deepest part of AABW from the ZM ($\varepsilon_{Nd} = -9$ to −9.6) is systematically less radiogenic than average CDW above ($\varepsilon_{Nd} = -8.5$, Figs. 4 and 6). The lower Nd isotopic values of AABW (neutral density $\gamma^n \sim 28.3$ kg/m^3) at stations 131 and 161 on the ZM ($\varepsilon_{Nd} = -9.5$ and −9.6, respectively) most likely reflect inputs from less radiogenic continental sources, such as East Antarctica. The Nd isotope composition of sedimentary deposits north of the Dronning Maud Land from the Zero Meridian to about 40° E ranges from $\varepsilon_{Nd} = -10$ to −17 (Roy et al., 2007; van de Flierdt et al., 2007) and is thus a potential source for an unradiogenic signature of AABW formed locally off East Antarctica. A similar influence of unradiogenic source rocks on AABW was already proposed by van de Flierdt et al. (2006) on the basis of ferromanganese nodule data from the Indian sector of the Southern Ocean. This hypothesis is further supported by the pathway of dense waters that form through brine rejection in the Amery Ice Shelf region and then flow westward within the Antarctic Slope Current (ASC) before they mix with WSBW near the Zero Meridian in the Weddell–Enderby Basin to form AABW (Heywood and King, 2002; Meijers et al., 2010; Orsi et al., 1999). Recent circulation studies at the East Antarctic shelf strongly suggest AABW formation at about 60° E (Meijers et al., 2010). In their work Meijers et al. (2010) observed recently ventilated (oxygen content > 240 μmol/kg) bottom waters on the continental slope just west of Prydz Bay, which flow west within the ASC and mix into the Weddell Gyre. Any direct mixing of AABW and NADW, which would also have a suitably low ε_{Nd} composition to cause the observed unradiogenic AABW signature, can be excluded due to the density contrast between NADW ($\gamma^n = 27.7$ kg/m^3 to 28.27 kg/m^3) and locally formed AABW ($\gamma^n >$ 28.3 kg/m^3). Given that the formation process of AABW involves admixture of saline shelf waters, a significant influence of Nd supplied from the Antarctic continent is consistent with the difference of the Nd isotope composition between AABW and CDW in the eastern Weddell Gyre. Apparently, release from suspended particles or boundary exchange processes (Lacan and Jeandel, 2005) provide a less radiogenic signature to seawater in this region. This is in agreement with the low Nd isotope composition at station 178, which is located above the continental slope of Antarctica on the Zero Meridian ($\varepsilon_{Nd} = -9.6$ to −8.6, Table 1, Fig. 4). The least radiogenic value is measured at 200 m depth, suggesting an unradiogenic Antarctic imprint on (sub)surface waters.

4.3.3. Is the Nd isotope composition of CDW only a result of mixing?

Piepgras and Wasserburg (1982) have previously shown that the overall Nd budget in average CDW is dominated by NADW and receives only small contributions from Pacific waters ($\varepsilon_{Nd} \approx -3.8$, 52 pmol/kg Piepgras and Jacobsen, 1988), which is general agreement in with the data from this study (Fig. 7). Our data suggest Atlantic contributions of 70–75% in the entire Atlantic sector of the Southern Ocean, whereas Piepgras and Wasserburg (1982) estimated a similar 50% to 70% contribution of Atlantic waters in the Drake Passage. As discussed before, scavenging north of the PF potentially removes Nd from the water column. In consequence, the Nd concentrations in the Southern Ocean should be somewhat too low to represent conservative mixing. This is indeed the case when the average composition of CDW is employed for the mixing calculation (Fig. 7, gray diamond). North of the PF the Nd concentration of CDW is clearly influenced by particle uptake and release in the entire water column, as mentioned above. At the stations within the WG and in the southern DP, however, these vertical processes obviously cease at intermediate (~1000 m in the WG) or greater (~3000 m at station 236) depths, as indicated by largely constant Nd concentrations suggesting that particle exchange processes do not alter these deep concentrations any more. The average Nd concentration of 25.1 (±1) pmol/kg at

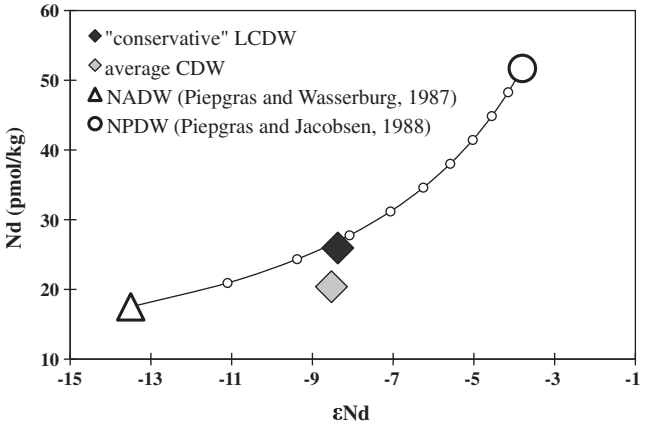

Fig. 7. Two-component Nd isotope mixing between NPDW ($\varepsilon_{Nd} = -3.8 \pm 0.3$; 55.7 pmol/kg; open circle) and NADW ($\varepsilon_{Nd} = -13.5 \pm 0.4$; 17.5 pmol/kg; open triangle) from Piepgras and Jacobsen (1988) and Piepgras and Wasserburg (1987), respectively. The mixing line is divided into 10% fractions (open circles). The "conservative" part of LCDW (black diamond) plots right on the mixing line, whereas mean CDW (gray diamond) plots somewhat below the mixing line.

these stations is therefore used as the "conservative" Nd concentration of LCDW. Applying this value for the mixing calculations shows that Nd in LCDW can be explained by a mixing of Pacific and Atlantic waters without any significant contributions from the Antarctic continent (black diamond, Fig. 7). These considerations also show that Nd is not only transported in dissolved form but to some extent also adsorbed to particles as a result of scavenging as discussed above (see also Piepgras and Jacobsen, 1988). Apparently, the particulate load largely re-dissolves within LCDW south of the ACC, where it generates the observed seemingly conservative Nd concentrations and isotope compositions of the LCDW.

4.4. The Hf–Nd isotopes and the seawater array

The combined Hf and Nd isotope compositions show that Southern Ocean waters are shifted toward more radiogenic Hf values compared to the "terrestrial array" (Fig. 8A and B). Similar to previous studies (Godfrey et al., 2009; Rickli et al., 2009, 2010; Zimmermann et al., 2009a,b), our data plots on or very near to the "seawater array" derived from ferro-manganese crusts and nodules (e.g. Albarède et al., 1998; David et al., 2001; van de Flierdt et al., 2006). Our samples form a narrow cluster located between Atlantic (Rickli et al., 2009) and Pacific seawater (Zimmermann et al., 2009a). The deep water data obtained in this study agree very well with the distribution of the ferromanganese nodule data from the same area (van de Flierdt et al., 2006) but are on average 1 ε-unit less radiogenic in their Nd isotope composition than the nodules (Fig. 8B). The most likely explanation is that ferromanganese crusts integrate the overlying seawater composition over several tens of thousands of years, suggesting that the observed Nd isotope compositions are a mixture of at least the past glacial and the present interglacial period. A more radiogenic signal of CDW and AABW in the past would therefore imply a stronger input of Pacific source waters (or a weaker Atlantic input) to the Southern Ocean during the last glacial period, which is consistent with high-resolution Nd isotope records from the Southern Ocean (e.g. Piotrowski et al., 2008). Such a difference is not observed for Hf isotopes, which suggests that the glacial/interglacial variability of dissolved Hf isotopes in seawater of the Southern Ocean was small.

All recent studies on the dissolved Hf and Nd isotope distribution in seawater including ours (Rickli et al., 2009, 2010; Zimmermann et al., 2009a,b) indicated that Hf isotopes are of limited use as tracer for (past) water mass and ocean circulation. Besides that they are more complicated to measure than Nd isotopes, they also show less variation between water masses reflecting either a long residence time or isotopically homogenous inputs of Hf to the sea.

Both elements exhibit only either small (Nd) or insignificant (Hf) variations in their isotope composition in the studied area. Continental inputs from Antarctica only significantly influence the Nd isotope composition of AABW, whereas this is not the case for Hf. The lack (Hf) or very low (Nd) continental input from Antarctica indicates that both isotope compositions are mainly governed by admixed contributions from the major ocean basins. For this reason, our results cannot contribute to the debate if the Hf budget in the world ocean is only governed by weathering inputs. The only supporting evidence comes from the lack of increased Hf concentrations at depths below 1500 m at station 113, where hydrothermal activity caused enhanced inputs of Mn and Fe (Klunder et al., 2011; Middag et al., 2011), which argues against significant hydrothermal contributions of Hf to seawater.

5. Conclusions

Samples from 14 full water depth stations in the Atlantic sector of the Southern Ocean were analyzed for their Hf and Nd isotope composition and concentration. The concentration patterns for both elements are similar to most particle reactive metals whereby the lowest values are observed in near surface waters with increasing values toward greater depths. However, there are distinct differences between the distributions of the two elements with respect to the gradients of change:

(1) The concentration patterns of Hf show low values in the upper water column and are elevated and nearly constant at greater depths. This suggests that scavenging of Hf by particles and subsequent release are finalized at shallow depths, resulting in a more nutrient like vertical distribution.
(2) The Nd concentrations at stations north of the Polar Front increase linearly throughout the entire water column implying scavenging at the surface and continuous release with depth, which points to different affinities of Hf and Nd to particles.

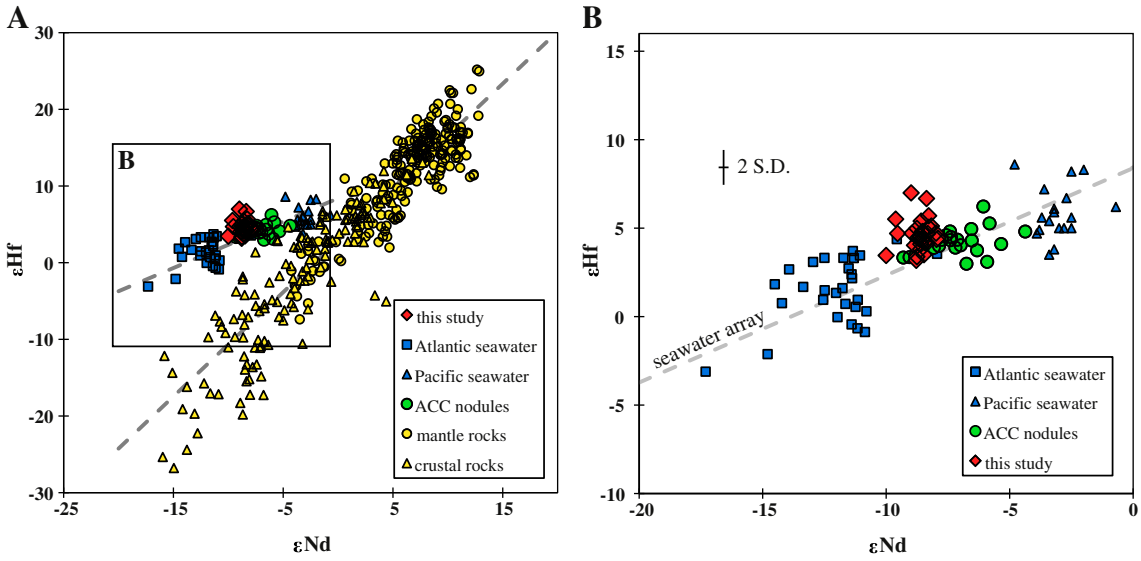

Fig. 8. Hafnium and Nd isotope systematics of terrestrial rocks (Vervoort et al., 1999; van de Flierdt et al., 2007), ferromanganese nodules from the Southern Ocean (van de Flierdt et al., 2006) and seawater (Rickli et al., 2009; Zimmermann et al., 2009a, this study) (A). Blow up (B) shows that the data from this study (red diamonds) plot between Atlantic (blue squares, Rickli et al., 2009) and Pacific compositions (blue triangles, Zimmermann et al., 2009a). The Hf isotope data agree well with the values obtained from ferromanganese nodules (green circles, van de Flierdt et al., 2006). The Nd data show less radiogenic values than obtained from these nodules, indicating a stronger Pacific influence during the last Glacial period.

(3) Unambiguous conclusions on differences in residence time between Hf and Nd cannot be drawn on the basis of our data given that variations in isotope compositions of the inputs of Hf to seawater to date remain largely unconstrained.
The isotope compositions of both elements do not show large variations within most of the ACC and in the Weddell Gyre, but some distinct features are observed:

(4) The Hf isotope compositions are remarkably constant and do not show any significant deviations from an average ε_{Hf} of 4.6 and no discernable differences between water masses documenting that Hf isotopes are not a useful tracer for present and past water masses in the studied area. The data agree well with previously measured ferromanganese nodule data. Combined Hf and Nd isotope values plot in a narrow cluster on the "seawater array" and are in agreement with ferromanganese deposits from this area (van de Flierdt et al., 2006). The Nd isotope data of the nodules are, however, on average about 1 ε unit more radiogenic, implying higher Pacific and lower Atlantic water mass contributions in the last glacial period. The Hf isotope data do not indicate such a shift and suggest that the glacial/interglacial variability of dissolved Hf isotopes in seawater of the Southern Ocean was small.

(5) AABW ($\varepsilon_{Nd} = -9$) is somewhat less radiogenic in its Nd isotope composition than CDW above ($\varepsilon_{Nd} = -8.5$) along the Zero Meridian, documenting continental inputs from the Antarctic continent during formation of AABW. However, the overall water column is mainly controlled by water mass mixing and thus potential continental inputs are not resolvable in the Nd (or Hf) isotope composition of CDW. The inflow of NADW is clearly reflected by less radiogenic Nd isotope signatures north of 50° S. Admixture of waters from the Agulhas Current is reflected by unradiogenic ε_{Nd} values near the surface close to South Africa.

(6) On a larger scale the Nd isotope composition of LCDW can be explained by a two component mixing of NPDW and NADW with a 70–75% contribution of the Atlantic-sourced waters.

Acknowledgments

This study was funded by a grant of the Deutsche Forschungsgemeinschaft (DFG) to M.F. (project FR1198/2) within the priority program "Antarctic Research" (*SPP* 1158). The authors would like to thank Jutta Heinze and Ana Kolevica for the priceless lab support and Folkmar Hauff and Anton Eisenhauer for providing assistance and machine time on the TIMS. We acknowledge Catherine Jeandel and Catherine Pradoux for providing the additional samples from ANTXXIII/3. Most importantly, we thank the chief scientists Eberhard Fahrbach and Hein de Baar, as well as Captain Stefan Schwarze and the crew of *Polarstern* for their contribution and braveness. Many thanks to Jan van Ooijen for the Si data and to Steven van Heuven to merge the ODV data. We acknowledge Celia Venchiarutti for her help during sample collection and preparation. This paper is dedicated to those, who did not return from expedition ANTXXIV/3.

Appendix A. Supplementary data

Supplementary data to this article can be found online at doi:10.1016/j.epsl.2011.11.025.

References

Albarède, F., Goldstein, S.L., 1992. Geology world map of Nd isotopes in sea-floor ferromanganese deposits. Geology 20, 761–763.
Albarède, F., Goldstein, S.L., Dautel, D., 1997. The neodymium isotopic composition of manganese nodules from the Southern and Indian oceans, the global oceanic neodymium budget, and their bearing on deep ocean circulation. Geochim. Cosmochim. Acta 61, 1277–1291.
Albarède, F., Simonetti, A., Vervoort, J.D., Blichert-Toft, J., Abouchami, W., 1998. A Hf-Nd isotopic correlation in ferromanganese nodules. Geophys. Res. Lett. 25 (20), 3895–3898.
Arsouze, T., Dutay, J.-C., Lacan, F., Jeandel, C., 2009. Reconstructing the Nd oceanic cycle using a coupled dynamical–biogeochemical model. Biogeosciences 6, 2829–2846.
Baars, O., Croot, P.L., 2011. The speciation of dissolved zinc in the Atlantic sector of the Southern Ocean. Deep Sea Res. Part II 58, 2720–2737.
Bau, M., Koschinsky, A., 2006. Hafnium and neodymium isotopes in seawater and in ferromanganese crusts: the "element perspective". Earth Planet. Sci. Lett. 241, 952–961.
Bayon, G., Vigier, N., Burton, K.W., Jean Carignan, A.B., Etoubleau, J., Chu, N.-C., 2006. The control of weathering processes on riverine and seawater hafnium isotope ratios. Geology 34, 433.
Boebel, O., Lutjeharms, J., Schmid, C., Zenk, W., Rossby, T., Barron, C., 2003. The Cape Cauldron: a regime of turbulent inter-ocean exchange. Deep-Sea Res. II Top. Stud. Oceanogr. 50, 57–86.
Byrne, R.H., 2002. Inorganic speciation of dissolved elements in seawater: the influence of pH on concentration ratios. Geochem. Trans. 3 (2), 11–16. doi:10.1039/b109732f.
Carmack, E., Foster, T., 1975. On the flow of water out of the Weddell Sea. Deep Sea Res. Oceanogr. Abstr. 22, 711–724.
Chu, N.-C., Taylor, R.N., Chavagnac, V., Nesbitt, R.W., Boella, R.M., Milton, J.A., German, C.R., Bayon, G., Burton, K., 2002. Hf isotope ratio analysis using multi-collector inductively coupled plasma mass spectrometry: an evaluation of isobaric interference corrections. J. Anal. At. Spectrom. 17, 1567–1574.
David, K., Frank, M., O'Nions, R.K., Belshaw, N.S., Arden, J.W., 2001. The Hf isotope composition of global seawater and the evolution of Hf isotopes in the deep Pacific Ocean from Fe-Mn crusts. Chem. Geol. 178, 23–42.
The expedition of the research vessel "Polarstern" to the Antarctic in 2008 (ANT-XXIV/3). In: Fahrbach, E., de Baar, H.J.W. (Eds.), Reports on Polar and Marine Research. Alfred-Wegener-Institute for Polar and Marine Research, p. 232http://hdl.handle.net/10013/epic.34050.
Firdaus, M.L., Norisuye, K., Nakagawa, Y., Nakatsuka, S., Sohrin, Y., 2008. Dissolved and labile particulate Zr, Hf, Nb, Ta, Mo and W in the western North Pacific Ocean. J. Oceanogr. 64, 247–257.
Firdaus, M.L., Minami, T., Norisuye, K., Sohrin, Y., 2011. Strong elemental fractionation of Zr–Hf and Nb–Taacross the Pacific Ocean. Nat. Geosci. 4, 227–230.
Frank, M., Reynolds, B.C., O'Nions, R.K., 1999. Nd and Pb isotopes in Atlantic and Pacific water masses before and after closure of the Panama gateway. Geology 27, 1147–1150.
Franzese, A.M., Hemming, S., Goldstein, S., Anderson, R., 2006. Reduced Agulhas leakage during the Last Glacial Maximum inferred from an integrated provenance and flux study. Earth Planet. Sci. Lett. 250, 72–88.
Georgi, D.T., 1981. On the relationship between the large-scale property variations and fine structure in the circumpolar deep water. J. Geophys. Res. 86, 6556–6566.
Godfrey, L.V., Field, M.P., Sherrell, R.M., 2008. The estuarine distributions of Zr, Hf and Ag in the Hudson River, and the implications for their continental and anthropogenic sources to seawater. Geochem. Geophys. Geosyst. 9, Q12007. doi:10.1029/2008GC002123.
Godfrey, L.V., Zimmermann, B., Lee, D.C., King, R.L., Vervoort, J.D., Sherrell, R.M., Halliday, A.N., 2009. Hafnium and neodymium isotope variations in NE Atlantic seawater. Geochem. Geophys. Geosyst. 10, Q08015. doi:10.1029/2009GC002508.
Gordon, A.L., 1971. Oceanography of Antarctic waters. In: Reid, J.L. (Ed.), Antarctic Research Series, pp. 169–203.
Halliday, N., Davidson, P., Owen, M., Olivarez, M., 1992. Metalliferous sediments and the scavenging residence time of Nd near hydrothermal vents. Geophys. Res. Lett. 19, 761–764.
Heywood, K.J., King, B.A., 2002. Water masses and baroclinic transports in the South Atlantic and Southern oceans. J. Mar. Res. 60, 639–676.
Jacobsen, S.B., Wasserburg, G.J., 1980. Sm–Nd isotopic evolution of chondrites. Earth Planet. Sci. Lett. 50, 139–155.
Jeandel, C., 1993. Concentration and isotopic composition of Nd in the South Atlantic Ocean. Earth Planet. Sci. Lett. 117, 581–591.
Jeandel, C., Bishop, J.K., Zindler, A., 1995. Exchange of neodymium and its isotopes between seawater and small and large particles in the Sargasso Sea. Geochim. Cosmochim. Acta 59, 535–547.
Kemp, A.I.S., Foster, G.L., Scherstén, A., Whitehouse, M.J., Darling, J., Storey, C., 2009. Concurrent Pb–Hf isotope analysis of zircon by laser ablation multi-collector ICP-MS, with implications for the crustal evolution of Greenland and the Himalayas. Chem. Geol. 261, 244–260.
Klatt, O., Fahrbach, E., Hoppema, M., Rohardt, G., 2005. The transport of the Weddell Gyre across the Prime Meridian. Deep-Sea Res. II Top. Stud. Oceanogr. 52, 513–528.
Klunder, M., Laan, P., Middag, R., de Baar, H.J.W., van Ooijen, J.C., 2011. Dissolved iron in the Southern Ocean (Atlantic sector). Deep Sea Res. Part II 58, 2678–2694.
Lacan, F., Jeandel, C., 2005. Acquisition of the neodymium isotopic composition of the North Atlantic Deep Water. Geochem. Geophys. Geosyst. 6, Q12008. doi:10.1029/2005gc000956.
Meijers, A.J.S., Klocker, A., Bindoff, N.L., Williams, G.D., Marsland, S.J., 2010. The circulation and water masses of the Antarctic shelf and continental slope between 30 and 80°E. Deep-Sea Res. II Top. Stud. Oceanogr. 57 (9–10), 723–737.
Middag, R., de Baar, H.J.W., Laan, P., Cai, P.H., van Ooijen, J.C., 2011. Dissolved manganese in the Atlantic sector of the Southern Ocean. Deep Sea Res. Part II 58, 2661–2677.
Münker, C., Weyer, S., Scherer, E., Mezger, K., 2001. Separation of high field strength elements (Nb, Ta, Zr, Hf) and Lu from rock samples for MC-ICPMS measurements. Geochem. Geophys. Geosyst. 2. doi:10.1029/2001GC000183.

Nachtrieb, N.H., Conway, J.G., 1948. The extraction of ferric chloride by isopropyl ether. I. J. Am. Chem. Soc. 70, 3547–3552.
Nachtrieb, N.H., Fryxell, R.E., 1948. The extraction of ferric chloride by isopropyl ether. II. J. Am. Chem. Soc. 70, 3552–3557.
Nowell, G.M., Kempton, P.D., Noble, S.R., Fitton, J.G., Saunders, A.D., Mahoney, J.J., Taylor, R.N., 1998. High precision Hf isotope measurements of MORB and OIB by thermal ionisation mass spectrometry: insights into the depleted mantle. Chem. Geol. 149, 211–233.
Orsi, A.H., Whitworth III, T., Nowlin, W.D., 1995. On the meridional extent and fronts of the Antarctic circumpolar current. Deep-Sea Res. I Oceanogr. Res. Pap. 42, 641–673.
Orsi, A.H., Johnson, G.C., Bullister, J.L., 1999. Circulation, mixing, and production of Antarctic Bottom Water. Prog. Oceanogr. 43, 55–109.
Orsi, A.H., Smethie Jr., W.M., Bullister, J.L., 2002. On the total input of Antarctic waters to the deep ocean: a preliminary estimate from chlorofluorocarbon measurements. J. Geophys. Res. 107, 3122. doi:10.1029/2001JC000976.
Patchett, P.J., White, W.M., Feldmann, H., Kielinczuk, S., Hofmann, A.W., 1984. Hafnium rare-earth element fractionation in the sedimentary system and crustal recycling into the Earth's mantle. Earth Planet. Sci. Lett. 69, 365–378.
Piepgras, D.J., Jacobsen, S.B., 1988. The isotopic composition of neodymium in the North Pacific. Geochim. Cosmochim. Acta 52, 1373–1381.
Piepgras, D.J., Wasserburg, G.J., 1982. Isotopic composition of neodymium in waters from the Drake Passage. Science 217, 207–214.
Piepgras, D.J., Wasserburg, G.J., 1987. Rare earth element transport in the western North Atlantic inferred from Nd isotopic observations. Deep Sea Res. Part B 51, 1257–1271.
Pin, C., Zalduegui, J.F.S., 1997. Sequential separation of light rare-earth elements, thorium and uranium by miniaturized extraction chromatography: application to isotopic analyses of silicate rocks. Anal. Chim. Acta 339, 79–89.
Piotrowski, A.M., Lee, D.-C., Christensen, J.N., Burton, K.W., Halliday, A.N., Hein, J.R., Gunther, D., 2000. Changes in erosion and ocean circulation recorded in the Hf isotopic compositions of North Atlantic and Indian Ocean ferromanganese crusts. Earth Planet. Sci. Lett. 181, 315–325.
Piotrowski, A., Goldstein, S., Hemming, S., Fairbanks, R., Zylberberg, D., 2008. Oscillating glacial northern and southern deep water formation from combined neodymium and carbon isotopes. Earth Planet. Sci. Lett. 272, 394–405.
Reid, J., Lynn, R., 1971. On the influence of the Norwegian-Greenland and Weddell seas upon the bottom waters of the Indian and Pacific oceans. Deep-Sea Res. 18, 1063–1088.
Rhein, M., Stramma, L., Send, U., 1995. The Atlantic Deep Western Boundary Current: water masses and transports near the equator. J. Geophys. Res. 100, 2441–2457.
Rickli, J., Frank, M., Halliday, A.N., 2009. The hafnium–neodymium isotopic composition of Atlantic seawater. Earth Planet. Sci. Lett. 280, 118–127.
Rickli, J., Frank, M., Baker, A.R., Aciego, S., de Souza, G., Georg, R.B., Halliday, A.N., 2010. Hafnium and neodymium isotopes in surface waters of the eastern Atlantic Ocean: implications for sources and inputs of trace metals to the ocean. Geochim. Cosmochim. Acta 74, 540–557.
Rohardt, G., 2009. Continuous thermosalinograph oceanography along Polarstern cruise track ANT-XXIV/3. http://doi.pangaea.de/10.1594/PANGAEA.727465.
Roman, R.E., Lutjeharms, J.R.E., 2010. Antarctic intermediate water at the Agulhas Current retroflection region. J. Mar. Syst. 81, 273–285.
Roy, M., van de Flierdt, T., Hemming, S.R., Goldstein, S.L., 2007. 40Ar/39Ar ages of hornblende grains and bulk Sm/Nd isotopes of circum-Antarctic glacio-marine sediments: implications for sediment provenance in the southern ocean. Chem. Geol. 244, 507–519.
Rutgers van der Loeff, M.M., Berger, G.W., 1993. Scavenging of ^{230}Th and ^{231}Pa near the Antarctic polar front in the South Atlantic. Deep-Sea Res. 40, 339–357.
Sarmiento, J.L., Simeon, J., Gnanadesikan, A., Gruber, N., Key, R.M., Schlitzer, R., 2007. Deep ocean biogeochemistry of silicic acid and nitrate. Global Biogeochem. Cycles 21 (GB1S90). doi:10.1029/2006GB002720.
Schlitzer, R., 2011. Ocean Data View. http://odv.awi.de.
SCOR Working Group, 2007. GEOTRACES — an international study of the global marine biogeochemical cycles of trace elements and their isotopes. Chem. Erde 67, 85–131.
Siddall, M., Khatiwala, S., van de Flierdt, T., Jones, K., Goldstein, S., Hemming, S., Anderson, R., 2008. Towards explaining the Nd paradox using reversible scavenging in an ocean general circulation model. Earth Planet. Sci. Lett. 274, 448–461.
Sievers, H.A., Nowlin, W.D., 1984. The stratification and water masses at Drake Passage. J. Geophys. Res. Oceans 89, 489–514.
Stramma, L., England, M., 1999. On the water masses and mean circulation of the South Atlantic Ocean. J. Geophys. Res. 104, 20863–20883.
Suga, T., Talley, D., 1995. Antarctic intermediate water circulation in the tropical and subtropical South Atlantic. J. Geophys. Res. 100, 13441–13453.
Tachikawa, K., Jeandel, C., Roy-Barman, M., 1999. A new approach to the Nd residence time in the ocean: the role of atmospheric inputs. Earth Planet. Sci. Lett. 170, 433–446.
Tachikawa, K., Athias, V., Jeandel, C., 2003. Neodymium budget in the modern ocean and paleo-oceanographic implications. J. Geophys. Res. Oceans 108, 3254. doi:10.1029/1999jc000285.
Tanaka, T., Togashi, S., Kamioka, H., Amakawa, H., Kagami, H., Hamamoto, T., Yuhara, M., Orihashi, Y., Yoneda, S., Shimizu, H., Kunimaru, T., Takahashi, K., Yanagi, T., Nakano, T., Fujimaki, H., Shinjo, R., Asahara, Y., Tanimizu, M., Dragusanu, C., 2000. JNdi-1: a neodymium isotopic reference in consistency with LaJolla neodymium. Chem. Geol. 168, 279–281.
Usbeck, R., Rutgers van der Loeff, M.M., Hoppema, M., Schlitzer, R., 2002. Shallow remineralization in the Weddell Gyre. Geochem. Geophys. Geosyst. 3. doi:10.1029/2001GC000182.
van de Flierdt, T., Frank, M., Lee, D.-C., Halliday, A.N., 2002. Glacial weathering and the hafnium isotope composition of seawater. Earth Planet. Sci. Lett. 201, 639–647.
van de Flierdt, T., Frank, M., Lee, D.-C., Halliday, A.N., Reynolds, B.C., Hein, J.R., 2004. New constraints on the sources and behavior of neodymium and hafnium in seawater from Pacific Ocean ferromanganese crusts. Geochim. Cosmochim. Acta 68, 3827–3843.
van de Flierdt, T., Hemming, S.R., Goldstein, S.L., Abouchami, W., 2006. Radiogenic isotope fingerprint of Wilkes Land–Adélie Coast Bottom Water in the circum-Antarctic Ocean. Geophys. Res. Lett. 33. doi:10.1029/2006GL026020.
van de Flierdt, T., Goldstein, S., Hemming, S., Roy, M., Frank, M., Halliday, A., 2007. Global neodymium–hafnium isotope systematics — revisited. Earth Planet. Sci. Lett. 259, 432–441.
Venchiarutti, C., Jeandel, C., Roy-Barman, M., 2008. Particle dynamics study in the wake of Kerguelen Island using thorium isotopes. Deep-Sea Res. I Oceanogr. Res. Pap. 55, 1343–1363.
Venchiarutti, C., Rutgers van der Loeff, M.M., Stimac, I., 2011. Scavenging of ^{231}Pa and thorium isotopes based on dissolved and size-fractionated particulate distributions at Drake Passage (ANTXXIV-3). Deep Sea Res. Part II 58, 2767–2784.
Vervoort, J.D., Patchett, P.J., Blichert-Toft, J., Albarède, F., 1999. Relationships between Lu–Hf and Sm–Nd isotopic systems in the global sedimentary system. Earth Planet. Sci. Lett. 168, 79–99.
Whitworth III, T., Nowlin, W.D., 1987. Water masses and currents of the Southern Ocean at the Greenwich Meridian. J. Geophys. Res. 92, 6462–6476.
Wüst, G., 1935. Schichtung und Zirkulation des Atlantischen Ozeans. Die Stratosphäre des Atlantischen Ozeans: Wissenschaftliche Ergebnisse der Deutschen Atlantischen Expedition auf dem Forschungs- und Vermessungsschiff "Meteor" 1925–1927, 6, pp. 109–288.
Yu, E.-F., Francois, R., Bacon, M.P., 1996. Similar rates of modern and last-glacial ocean thermohaline circulation inferred from radiochemical data. Nature 379 (6567), 689–694.
Zimmermann, B., Porcelli, D., Frank, M., Rickli, J., Lee, D.C., Halliday, A.N., 2009a. The hafnium isotope composition of Pacific Ocean water. Geochim. Cosmochim. Acta 73, 91–101.
Zimmermann, B., Porcelli, D., Frank, M., Andersson, P.S., Baskaran, M., Lee, D.C., Halliday, A.N., 2009b. Hafnium isotopes in Arctic Ocean water. Geochim. Cosmochim. Acta 73, 3218–3233.